Check for updates

Discrete component model to explain the photophysics of bay-functionalized perylene bisimide derivatives

Chenbo Meng [ID] and Siegfried Eigler [ID] *

Bay functionalization of perylene bisimides (PBIs) is a widely used strategy to tailor their electronic structure. However, most bay-functionalized PBIs are symmetric, bearing identical substituents. Here, we present an asymmetrically functionalized PBI with distinct groups at the bay positions. The introduction of an aldehyde intermediate at the bay positions enables stepwise formation of benzimidazole (Imi) and dicyanoethylene (DCE) moieties. In the resulting asymmetric mono-Imi-mono-DCE-PBI, Imi and DCE act as electron-donating and electron-withdrawing groups, respectively. Comparing its spectral features with symmetric di-Imi-PBI and di-DCE-PBI reveals that its absorption spectrum is dominated by the DCE group, while emission is governed by the Imi group. The photoluminescence quantum yield (PLQY) of this asymmetric PBI lies between di-Imi-PBI and di-DCE-PBI. Furthermore, acid titration of di-Imi-PBI yielded another asymmetric PBI through one-sided protonation. Unlike mono-Imi-mono-DCE-PBI, this partially protonated derivative shows the lowest PLQY value compared with its symmetric counterparts. Theoretical calculations provided molecular orbital energy levels of the PBI core and bay substituents. Applying a discrete component model, we rationalized the photo-induced charge transfer (PICT) behavior. This analysis shows that additional electron transfer from the PBI core to the benzimidazolium (Imi+) moiety in the protonated derivative accounts for the pronounced fluorescence quenching observed.

Introduction

Perylene bisimide (PBI) has attracted interest from both academia and industry due to its distinctive photophysical properties, which are particularly promising for applications in photovoltaics[1,2] and photocatalysis.[3,4] The π-conjugated perylene core functions as the primary chromophore, enabling the light absorption in the 350–450 nm range, which corresponds to UVA and violet-blue regions. The introduction of imide groups has been demonstrated to result in a shift of the absorption to longer wavelengths beyond 500 nm.[5] However, the tunability is greatly restricted even with the variation in the side-chain structures attached to the imide groups. This limitation arises from the node at the nitrogen atom in both the highest occupied molecular orbital (HOMO) and lowest unoccupied molecular orbital (LUMO).[6] As a result, the electronic communication between side chains and the perylene core is significantly hindered. Therefore, the chemical modifications to the side chain of the imide group exert little influence on the electronic transition of PBI molecules.

Beyond imide substitution, an alternative approach to tune the electronic structure of PBIs involves the functionalization at the perylene core itself. The peripheral carbon–hydrogen (C–H) σ bonds, particularly those at the bay positions, are more reactive toward electrophilic aromatic substitution than other sites of the molecular structure. In 1995, BASF was granted a patent for the bromination on the perylene core,[7] after which research into perylene functionalization rapidly increased. This bromination protocol remains one of the most widely employed methods, with minor modifications over the years.[8–11] From the brominated precursor, various heteroatoms can be introduced at the bay positions to generate a wide range of functional groups, including ethers, thiols and amines.[12] In addition, a series of carbon–carbon (C–C) coupling reactions enable the extension of the conjugated π-system, becoming a popular strategy for perylene chemistry. For example, di-aryl-functionalized PBIs can be synthesized *via* Suzuki coupling between di-brominated PBI and substituted phenylboronic acids.[13,14] The aryl substituents introduced through this method can bear a variety of functional groups, which extend outward from the PBI core. These pendant groups exert mesomeric effects, allowing for modulation of the photophysical properties depending on the electronic nature of the substituents. In a systematic study, Sivamurugan *et al.* explored the influence of substituents at bay-positions on the photophysical behaviour of di-aryl-functionalized PBIs.[15,16] It was reported that electron-donating groups, such as the methoxy group, induced a red shift to the

Institut für Chemie und Biochemie (SupraFAB), Freie Universität Berlin (FU-Berlin), Altensteinstraße 23A, 14195 Berlin, Germany. E-mail: siegfried.eigler@fu-berlin.de

absorption maximum (λ_{max}^{abs}) and significantly quenched fluorescence emission. In contrast, electron-withdrawing groups like the trifluoromethyl group had a comparatively modest impact on the spectrum. The authors attributed these spectral changes to charge transfer (CT) from electron-rich substituents to the electron-deficient PBI core, a phenomenon observed only with electron-donating groups at bay positions.

Most di-aryl-functionalized PBIs studied to date are symmetric, featuring identical substituents at the bay positions.[13,14] In contrast, fewer investigations have focused on asymmetric bay-functionalized PBIs. Hudhomme *et al.* demonstrated that the high reactivity of di-brominated PBI precursors made it less likely to form asymmetric PBIs *via* common Suzuki coupling protocols.[17] Instead, the reaction typically yielded the symmetric di-aryl-functionalized PBI and recovered unreacted di-brominated starting materials. Despite the rare examples for asymmetric di-aryl-functionalized PBIs, successful syntheses of asymmetric PBIs with distinct functional groups at the bay positions have been reported. 1-Cyano-7-piperidinyl PBI was synthesized by Chen *et al.*[18] In their study, theoretical simulations predicted that the combination of electron-withdrawing (cyano) and electron-donating (piperidinyl) groups would generate an intramolecular dipole across the perylene core. However, no direct comparison was made, especially in terms of spectral change, between this asymmetric PBI and its symmetric counterparts, thereby without common conclusions about the effect of asymmetry on photophysical properties. More than a decade ago, Würthner *et al.* conducted a comparative study on symmetric and asymmetric PBIs functionalized at the bay positions.[19] Their work examined bay-functionalized PBIs derivatives bearing 2,2′-biphenoxy and two individual phenoxy groups. Although these substituents differed in functionality, the resulting PBIs exhibited largely similar electronic structures. The only notable difference was a variation in core rigidity between the symmetric and asymmetric analogues. Nonetheless, this fundamental research aroused our interest in exploring the effects of asymmetric bay substitution, in particular with substituents exhibiting distinctive electronic structures, on the absorption and emission behaviour of functionalized PBIs.

Previous studies on asymmetric PBIs have suggested that the emergence of a CT absorption band may result from CT through the perylene core, from an electron-donating to an electron-withdrawing substituent at the bay position.[20] Such a CT process is expected to manifest as red-shifted absorption features.[17] However, many of these investigations have employed tertiary amines,[17] which are strong electron donors, as bay-position substituents. These groups inherently promote CT to the electron-deficient PBI core, even in the absence of a corresponding electron acceptor at the opposite bay position.[13,14] This intrinsic donor-to-core CT complicates the interpretation of spectroscopic data from asymmetric PBIs, as it becomes difficult to isolate and identify CT from donor to acceptor through the core. This obscures distinctions between donor-to-core and donor-to-acceptor CT pathways. Therefore, to enable a more precise investigation of asymmetric PBIs and to conclude on their CT behaviour, we designed a new system. This system is anticipated to get rid of interference from the strong electron-donating groups. This would facilitate a clearer

attribution of spectral features to specific CT mechanisms, offering deeper insight into structure–property relationships in functionalized PBIs.

To this end, we learned from a donor–acceptor system based on diaminodicyanoquinodimethane derivatives,[21] which bear a benzimidazole moiety as the donor and a dicyanomethylene group as the acceptor. These groups were in this study introduced at bay positions of PBIs with aryl spacers in between. With this strategy, an asymmetric PBI and its two symmetric counterparts were successfully synthesized. A comparative analysis of their absorption and emission spectra revealed distinct differences in their photophysical properties. Moreover, the protonation of the benzimidazole moiety enables the transformation from the donor into an acceptor unit, thus facilitating the formation of an additional asymmetric PBI. Based on theoretical calculations, we proposed a discrete component model to better describe the CT behaviour and photophysics for asymmetrically di-functionalized PBIs at the bay positions.

Results and discussion

Synthesis

1,7-Di-brominated PBIs (di-Br-PBI) were used as precursors to synthesize both symmetrically and asymmetrically functionalized PBIs. As shown in Fig. 1, the synthesis of di-Br-PBI followed a literature-reported method,[11] starting from commercially available perylenetetracarboxylic dianhydride (PTCDA). The reaction of PTCDA with cyclohexylamine (step i) afforded the corresponding PBI. The subsequent bromination with Br_2 (step ii) was carried out under reflux in dichloromethane (DCM) for five days, resulting in a mixture of di-brominated isomers (1,6- and 1,7-dibrominated PBIs; the atomic numbering shown in the structure of di-Br-PBI in italics), with the undesired 1,6-isomer comprising approximately 20–30% of the product mixture. To isolate the purified 1,7-isomers, the crude product was dispersed in a defined volume of DCM and stirred for 10 min. The solvent volume is crucial for the effective separation of 1,7-isomers from mixtures (see SI for details, Fig. S1). In this specific volume of solvents, the 1,6-isomers remain in the supernatant, while the pure 1,7-isomers precipitate as sediments. The sediment could be collected after centrifugation or filtration. Repeating this process can reduce the proportion of the 1,6-isomer to about 5%, as confirmed by proton nuclear magnetic resonance (^{1}H NMR) spectroscopy. Different from the commonly used recrystallization procedure,[8] which typically requires several days, this approach enables the rapid isolation of regioisomerically pure 1,7-di-Br-PBI within approximately one hour and in a high yield.

With the pure 1,7-regioisomer di-Br-PBI in hand, aldehyde groups were introduced by a Suzuki reaction with 4-formyl-phenylboronic acid (step iii). The resulting PBI with aldehyde groups at the bay positions (di-CHO-PBI) served as an intermediate for further functionalization. Subsequent reactions of di-CHO-PBI with *o*-phenylenediamine[22] (step iv) and malononitrile[17,23] (step v) led to the formation of benzimidazole (Imi)-functionalized PBI (di-Imi-PBI) and dicyanoethylene (DCE)-functionalized PBI (di-DCE-PBI), respectively. Using this approach, two symmetrically bay-
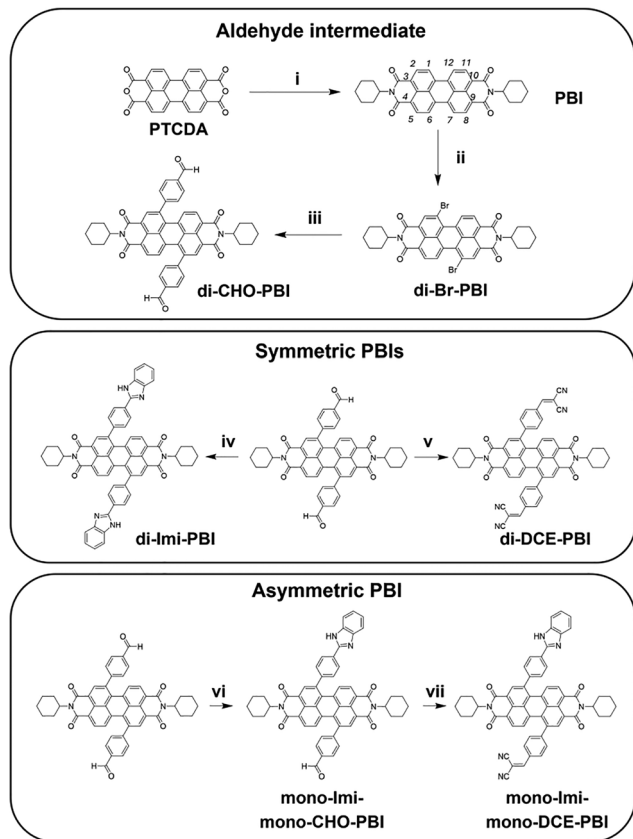
This journal is © the Owner Societies 2025

Phys. Chem. Chem. Phys., 2025, **27**, 23348–23355 | **23349**

Fig. 1 Reaction schemes for PBI derivatives: (i) cyclohexylamine, 155 °C, in DMF, 4.5 h, 97%; (ii) Br$_2$, reflux, in DCM, 5 days, 30%; (iii) 4-formylphenylboronic acid, K$_2$CO$_3$, Pd(PPh$_3$)$_4$, overnight reflux, in THF/H$_2$O (v/v = 4 : 1), 85%; (iv) o-phenylenediamine, KI, 80 °C, in DMF/H$_2$O (v/v = 9 : 1), 3 days, 49%; (v) malononitrile, triethylamine, 80 °C, in toluene, 3 h, 43%; (vi) o-phenylenediamine, KI, 80 °C, in DMF/H$_2$O (v/v = 9 : 1), 4 days, 10%; (vii) malononitrile, triethylamine, 80 °C, in toluene, 3 h, 98%.

functionalized PBIs were successfully synthesized: di-Imi-PBI, featuring electron-donating Imi moieties, and di-DCE-PBI, with electron-withdrawing DCE groups.

To synthesize the asymmetric mono-Imi-mono-DCE-PBI, a stepwise reaction strategy was employed. The reaction between di-CHO-PBI and o-phenylenediamine (step vi) was performed first. Notably, o-phenylenediamine must be added not only in stoichiometric amounts, but also in a controlled, stepwise manner to suppress the formation of the symmetric di-Imi-PBI as byproduct. With this method, mono-Imi-mono-CHO-PBI was successfully obtained in 10% yield. Subsequently, the reaction between mono-Imi-mono-CHO-PBI and malononitrile (step vii) afforded the final product, mono-Imi-mono-DCE-PBI. In the structure of mono-Imi-mono-DCE-PBI, the electron-donating Imi moiety and the electron-withdrawing DCE moiety are incorporated on the opposite sides of the bay positions of the PBI core.

Photophysical measurements

Solutions in DCM at the concentration of 10^{-6} M of di-Imi-PBI, di-DCE-PBI and mono-Imi-mono-DCE-PBI were prepared. This

concentration falls within the linear range of the absorbance-concentration relationship (see Fig. S2), which indicates the formation of molecular solutions, and thus the recorded spectra are related to the molecular behaviour of these PBI derivatives.

Fig. 2(a) shows normalized absorption spectra in the visible light range (400–800 nm). In this region, the absorption peaks correspond to the ground state (S$_0$) to first excited state (S$_1$) transition (S$_0$–S$_1$) for PBI-based molecules.[24,25] Unlike the unsubstituted PBI at bay positions, all three compounds exhibit a substantial loss of vibronic progression, resulting in broadened and partially overlapping peaks. Among them, the absorption spectrum of di-Imi-PBI displays the least pronounced vibronic features. In addition, bay functionalization induces a red shift of the absorption maxima (λ_{max}^{abs}) relative to the unsubstituted PBI, with the magnitude of the shift depending on the nature of bay substituents. As summarized in Table 1, di-Imi-PBI shows λ_{max}^{abs} at 557 nm, corresponding to a red shift of 34 nm compared to the unsubstituted PBI. Mono-Imi-mono-DCE-PBI exhibits λ_{max}^{abs} at 548 nm (with a red shift of 25 nm), while di-DCE-PBI has λ_{max}^{abs} at 546 nm (with a red shift of 23 nm). The comparison of the absorption spectra of di-DCE-PBI and mono-Imi–mono-DCE-PBI reveals that their absorption maxima are nearly identical, suggesting that structural symmetry has little influence on this spectral feature. In this case, substitution of one DCE group with an Imi moiety does not significantly alter λ_{max}^{abs}. This observation further indicates that the vibronic characteristics of the asymmetric PBI are primarily determined by the electron-withdrawing group at the bay position, whereas the electron-donating moiety plays a negligible role in shaping the absorption profile.

Fig. 2(b) shows their normalized fluorescence spectra. Di-DCE-PBI exhibits the shortest λ_{max}^{em}, centred at 596 nm. Di-Imi-PBI displays λ_{max}^{em} at 633 nm, which is only 5 nm longer than that of mono-Imi-mono-DCE-PBI at 628 nm. In addition, the spectral shape of mono-Imi-mono-DCE-PBI closely resembles that of di-Imi-PBI, both showing broader emission bands. In other words, it has little effect on the emission spectrum when replacing one Imi group with a DCE moiety. This observation suggests that λ_{max}^{em} of the asymmetric PBI is mainly governed by the electron-donating group at the bay position, rather than the electron-withdrawing group. This correlation contrasts with the absorption properties described above, where λ_{max}^{abs} of the asymmetric PBI is primarily determined by the electron-withdrawing group.
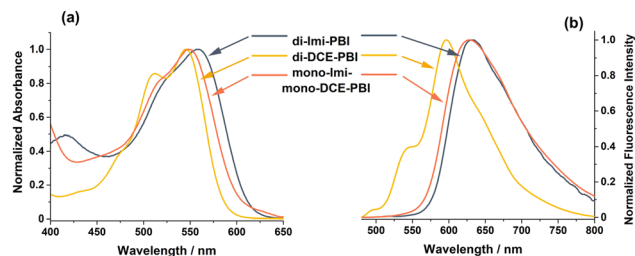

Fig. 2 Normalized (a) absorption spectra and (b) fluorescence spectra of di-Imi-PBI, di-DCE-PBI and mono-Imi–mono-DCE-PBI in DCM. Concentration: 10^{-6}–10^{-5} M.

23350 | *Phys. Chem. Chem. Phys.*, 2025, **27**, 23348–23355

This journal is © the Owner Societies 2025

Table 1 The photophysical properties of di-Imi-PBI, di-DCE-PBI and mono-Imi-mono-DCE-PBI, compared with unsubstituted PBI

Compound	λ_{max}^{abs}/nm	λ_{max}^{em}/nm	Stokes shift/cm^{-1}	PLQY[a]
PBI	524	533	322	1.00
di-Imi-PBI	557	633	2055	0.52
di-DCE-PBI	546	596	1536	0.83
mono-Imi-mono-DCE-PBI	548	628	2324	0.59

[a] The relative values of PLQY were calculated by using the unsubstituted PBI (PLQY = 1) as reference. See Section V in SI for details.

Furthermore, by considering both the absorption and emission spectra, the Stokes shift can be determined. Because λ_{max}^{abs} and λ_{max}^{em} of the asymmetric PBI are influenced by bay substituents in different fashions, its Stokes shift becomes more distinguished from its two symmetric counterparts. Specifically, the combination of a shorter λ_{max}^{abs} and a longer λ_{max}^{em} gives rise to the largest Stokes shift among the three compounds. As shown in Table 1, the asymmetric mono-Imi-mono-DCE-PBI has a Stokes shift of 2324 cm^{-1}, which exceeds those of the symmetric di-DCE-PBI (1536 cm^{-1}) and di-Imi-PBI (2055 cm^{-1}). Despite this pronounced Stokes shift, the photoluminescence quantum yield (PLQY) of the asymmetric PBI remains moderate, with a value of 0.59. In contrast, the PLQYs of di-Imi-PBI and di-DCE-PBI are 0.52 and 0.83, respectively. These results indicate that the asymmetric functionalization of PBI at the bay positions can substantially increase the Stokes shift without remarkably compromising the PLQY.

Titration assay

As already discussed, λ_{max}^{abs} and λ_{max}^{em} of the asymmetric PBI are primarily related to the electron-withdrawing and electron-donating groups at the bay position, respectively. Building on this insight, a conversion between an electron-donating and an electron-withdrawing group at the bay positions is anticipated to further elucidate the effect of bay substitutes on the photophysical properties of the bay-functionalized PBIs. Given the capability of being protonated, allowing conversion of an electron-donating to a positively charged, electron-withdrawing species, di-Imi-PBI was chosen for an acid titration assay. In this assay, *p*-toluenesulfonic acid (PTSA) and trifluoroacetic acid (TFA), representative of acids with different strengths, were used for protonation. The titration assay was conducted in two aprotic solvents with different polarities: chloroform (CHCl₃) and dimethyl sulfoxide (DMSO). For a quantitative assessment of this thermodynamic process, the molar ratio of acid to di-Imi-PBI, denoted as R, is defined as follows:

$$R = \frac{n_{acid}}{n_{di\text{-}Imi\text{-}PBI}}$$

Fig. 3(a) and (b) present a series of absorption and emission spectra, respectively, which were recorded during the titration assay for PTSA/CHCl₃ system. At lower acid concentrations ($R < 1$), λ_{max}^{abs} and λ_{max}^{em} remained unchanged compared with the neutral di-Imi-PBI, appearing at 562 nm and 636 nm, respectively. Upon further
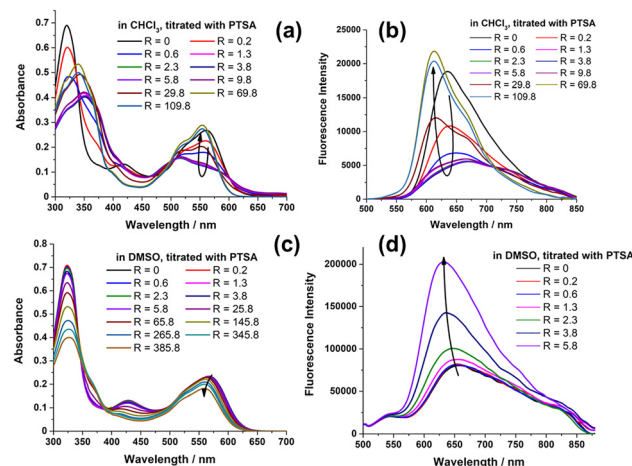

Fig. 3 A series of spectra collected during the acid titration by PTSA: (a) absorption spectra and (b) emission spectra in CHCl₃, (c) absorption spectra and (d) emission spectra in DMSO. All the emission spectra were recorded by the excitation wavelength at 470 nm.

acid addition ($R = 1.3$), the main peak in the original absorption spectrum evolved into a shoulder, while a new absorption band at 517 nm emerged. In this range ($0 < R < 1.3$), the fluorescence showed a significant decline. In the medium range ($1 < R < 29.8$), both absorption and emission spectra almost overlapped. When R exceeded 29.8, however, the intensities of both spectra started to differentiate, in which the fluorescence intensity increased strongly. Under these conditions, shifts of λ_{max}^{abs} and λ_{max}^{em} were observed. In the absorption spectra, λ_{max}^{abs} shifted to 554 nm, corresponding to a blue shift relative to the starting di-Imi-PBI (at 561 nm). In the emission spectra, λ_{max}^{em} shifted to 612 nm, also a blue shift compared to di-Imi-PBI (at 635 nm). With further acid addition, the spectral shapes remained unchanged, and the intensities decreased proportionally due to dilution effects rather than continuous protonation.

Fig. 3(c) and (d) show the absorption and emission spectra collected during the titration assay with PTSA in DMSO. In contrast to the remarkable spectral changes observed in CHCl₃, the spectra in DMSO exhibited only minor variations throughout the titration. Specifically, both λ_{max}^{abs} and λ_{max}^{em} underwent a gradual but slight blue shift as the amount of acid increased, without the significant changes in spectral shape. Nevertheless, as shown in Fig. 3(d), the fluorescence intensity increased progressively with the acid addition. At higher acid concentrations, the fluorescence became so strong that instrumental parameters had to be adjusted to keep the signal within the measurable range (see Fig. S3).

The same titration assays were conducted with TFA in both solvents. Fig. 4(a) and (b) show the corresponding absorption and emission spectra measured in CHCl₃, respectively. In the absorption spectra, a blue shift of λ_{max}^{abs} from 561 nm to 555 nm was observed across the entire investigated range of R values. However, different from the titration with PTSA, the overall spectral change with TFA was less significant, especially regarding the absorption intensity in the visible light region (400–700 nm). As for the emission spectra, the peak at λ_{max}^{em} exhibited an obvious

This journal is © the Owner Societies 2025

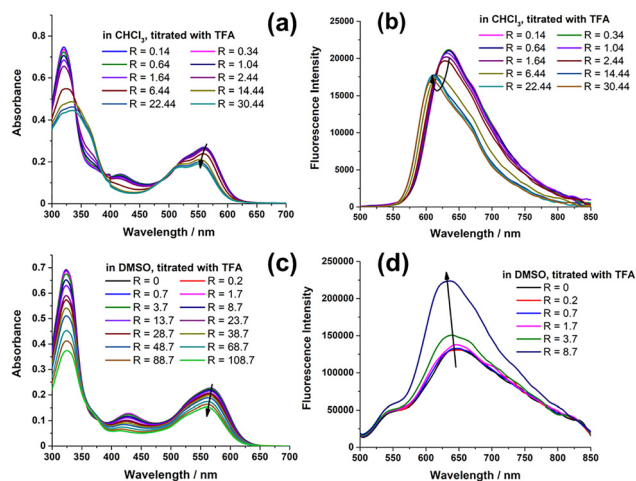*Phys. Chem. Chem. Phys.*, 2025, **27**, 23348–23355 | **23351**

Fig. 4 A series of spectra collected during the acid titration by TFA: (a) absorption spectra and (b) emission spectra in CHCl₃, (c) Absorption spectra and (d) emission spectra in DMSO. All the emission spectra were recorded by the excitation wavelength at 470 nm.

blue shift relative to the neutral di-Imi-PBI, from 634 nm to 611 nm after titration. Fig. 4(c) and (d) show the spectra obtained during the similar titration assay with TFA in DMSO. As shown in Fig. 4(c), λ_{max}^{abs} underwent only a slight blue shift from 567 nm to 563 nm without significant changes in the overall visible light region. In the emission spectra, as shown in Fig. 4(d), the fluorescence intensity increased substantially throughout the titration. For $R > 8.7$, the instrumental settings had to be adjusted to accommodate this marked increase in emission intensity (see Fig. S4). Similar to the spectral change observed in CHCl₃, the titration in DMSO also resulted in a gradual blue shift of λ_{max}^{em}.

As above demonstrated, the overall tendency of spectral change is clear. Both λ_{max}^{abs} and λ_{max}^{em} show a blue shift upon acid titration, regardless of the acid type or solvent. This observation is consistent with the expectation that the electron-donating Imi moieties in di-Imi-PBI are converted into electron-withdrawing benzimidazolium (Imi⁺) groups upon protonation. Like di-DCE-PBI, the positively charged Imi⁺ group, but an even more electron-deficient group than the DCE group, at the bay positions results in the blue-shifted absorption and emission compared to the neutral di-Imi-PBI. Although this conversion of functional groups accounts for the blue shift, some additional spectral features cannot be simply explained on this basis. For example, it is noteworthy that two sets of isosbestic points (at 508 nm and 600 nm, followed by 500 nm and 583 nm as R increases) are observed in the absorption spectra collected during the titration with PTSA in CHCl₃, as indicated in Fig. 3(a). The presence of multiple isosbestic points suggests that more than one equilibrium process is involved in the titration.[26,27] Theoretically, the two identical Imi groups at two opposite bay positions of di-Imi-PBI could undergo stepwise protonation, potentially forming an intermediate species in which one Imi group is protonated to form an Imi⁺ moiety while the other remains unprotonated. However, no direct evidence has yet been obtained to confirm

that the formation of this partially protonated intermediate accounts for one of the observed equilibria.

From another perspective, this partially protonated intermediate is indeed an asymmetric PBI derivative. As discussed above, it is suggested that the asymmetric PBI, like mono-Imi-mono-DCM-PBI, has a moderate value of the PLQY between its two symmetric counterparts, namely higher than that of the symmetric one with two electron-donating groups and lower than that of the one with two electron-withdrawing groups (see in Table 1). Based on this finding, the PLQY of PBI derivative is expected to gradually increase over the whole titration range, reflecting the stepwise conversion from di-Imi-PBI to a fully protonated species via a partially protonated asymmetric intermediate. To investigate the possible formation of such an asymmetric intermediate during titration, the PLQYs were calculated and plotted as a function of the R value, as shown in Fig. 5. Specifically, Fig. 5(a) presents the evolution of the PLQYs during the titration with PTSA, while Fig. 5(b) shows the corresponding result obtained with TFA. As expected, the PLQYs exhibit an almost linear increase with acid concentration for both acids in DMSO, supporting the hypothesis of a smooth transition through intermediates. However, in CHCl₃, the behaviour deviates notably from this trend. In the case of titration with PTSA, the PLQY initially decreases sharply upon the addition of a small amount of acid and then plateaus in the range of $0.5 < R < 5$ (see inset of Fig. 5(a)). Beyond $R = 10$, the PLQY increases rapidly and eventually levels off at a relatively high value of 0.76 when R exceeds 70. In contrast, during TFA titration in CHCl₃ (Fig. 5(b)), no clear increase in PLQY is observed following the initial sharp drop. Even after the addition of more than 200 equivalents of acid, the PLQY remains relatively unchanged over a wide range of R values ($25 < R < 250$). This plateau-like behaviour reflects on the level-off stage observed during the PTSA titration at low R values ($0.5 < R < 5$), but in this case, it keeps stable without further evolution.
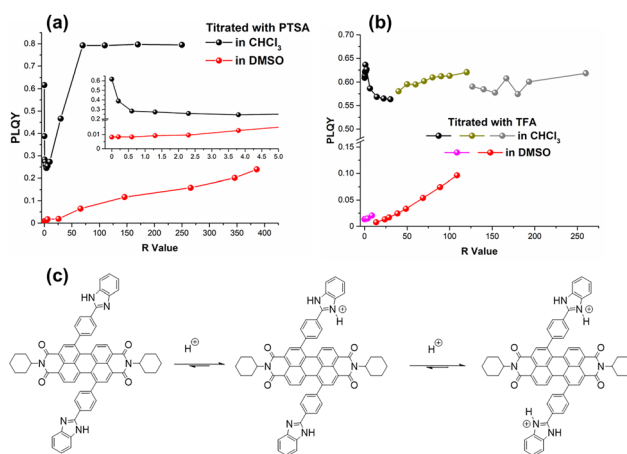

Fig. 5 Photoluminescence quantum yield (PLQY) evolution with the addition of acids: (a) titrated with PTSA in CHCl₃ and DMSO. Inset: The enlarged plot in the lower R value range, (b) titrated by TFA. The plots in different colors refer to the different batches of titration assays. Note that the original spectral data can be found in Fig. 3, 4 and Fig. S3–S5. (c) The possible structures involved in the stepwise protonation of di-Imi-PBI.

23352 | *Phys. Chem. Chem. Phys.*, 2025, **27**, 23348–23355

This journal is © the Owner Societies 2025

It can be implied that the protonation behaviour of di-Imi-PBI is strongly dependent on the combination of acid and solvent. In any given solvent, PTSA has a lower pK_a value than TFA. Consequently, Imi groups can be more easily protonated by PTSA than TFA. In addition, acid dissociation is promoted in polar solvents such as DMSO but suppressed in less polar solvents like CHCl$_3$. Therefore, among the conditions examined, PTSA in DMSO is expected to provide the greatest availability of free protons, followed by TFA in DMSO and PTSA in CHCl$_3$. TFA in CHCl$_3$ would be expected to release free protons with the greatest difficulty during the titration assay.

After comparing the acid dissociation capabilities of different acid/solvent combinations, it could be assumed that stepwise protonation is probably assessable, as evidenced by distinguished photophysical behaviours observed during the acid titration in these systems. For TFA/CHCl$_3$, fewer protons are released, and the equilibrium favours the formation of the partially protonated intermediate. In contrast, for PTSA/CHCl$_3$, more protons can be dissociated than in TFA/CHCl$_3$, enabling the equilibrium to further shift towards the fully protonated PBI species. These two possible equilibria are shown in Fig. 5(c). Considering the different dissociation abilities of PTSA and TFA in CHCl$_3$, it can be proposed that the stages corresponding to $0.5 < R < 5$ in PTSA/CHCl$_3$ and the stage with $R > 70$ in TFA/CHCl$_3$ represent conditions where the partially protonated PBI derivatives are the dominant species.

As for the titration in DMSO, owing to the strong tendency of proton dissociation from both acids, their addition preferentially leads to complete protonation without too much accumulation of partially protonated intermediates. This results in the direct formation of the fully protonated species, which exhibit higher PLQYs. Consequently, the PLQY shows an almost linear dependence on acid addition, as expected. As above mentioned, the stage where the PLQY keeps stable at its minimum over a broad range of acid content likely refers to the formation of asymmetric PBI species with only one-side protonation. Notably, the PLQY observed in this stage is even lower than that of the unprotonated di-Imi-PBI with two electron-donating Imi groups. However, the observation appears to contradict our earlier finding that the asymmetric PBI derivative exhibits the moderate PLQY between its two symmetric counterparts. To address this inconsistency, theoretical calculations are conducted, and the photo-induced charge transfer (PICT) behaviour will be discussed in the following section.

Photo-induced charge transfer (PICT) study based on theoretical calculations

To elucidate the relationship between the photophysical properties and the nature of bay substituents, theoretical calculations, using density functional theory (DFT), were performed. Based on the optimized geometries, the molecular orbital energies at HOMO and LUMO levels were compared. Fig. 6 shows the electronic distributions of these bay-functionalized PBI derivatives derived from molecular orbital analysis, in which HOMO levels are displayed as the bottom images and the LUMO levels as the top images. For clarity, the partially protonated di-Imi-PBI
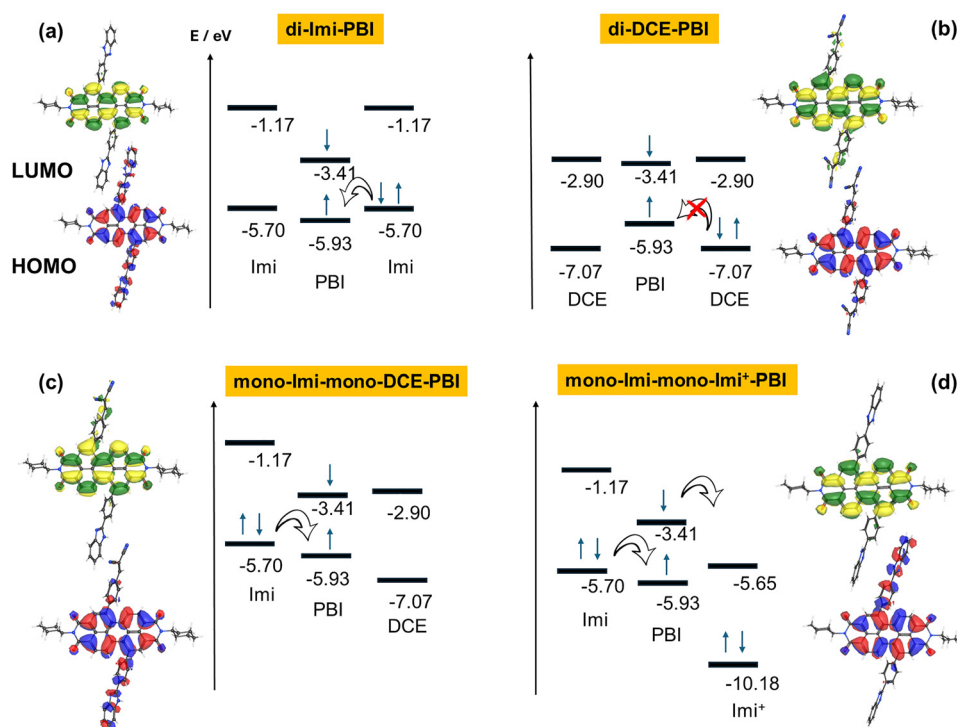

Fig. 6 The electronic structures of (a) di-Imi-PBI, (b) di-Imi-PBI, (c) mono-Imi-mono-DCE-PBI and (d) mono-Imi-mono-Imi⁺-PBI at HOMO (bottom image) and LUMO (top image) levels. In each figure, there is also a schematic diagram to illustrate the possible pathway (shown as curved black arrows) for charge transfer (CT). The two black bands represent the HOMO and LUMO energy levels, with the energy (E) unit of eV.

This journal is © the Owner Societies 2025

Phys. Chem. Chem. Phys., 2025, **27**, 23348–23355 | **23353**

is denoted here as mono-Imi-mono-Imi$^+$-PBI. At the HOMO level, the electron density around the electron-donating Imi moiety is higher than that around the electron-withdrawing groups, including DCE and Imi$^+$ groups. However, at the LUMO levels, the electrons are mainly localized on the PBI core, and the electron density around the Imi moiety becomes much lower. This variation in electron distribution suggests that the intra-molecular charge transfer (ICT) from the Imi moiety to the PBI core occurs during the electronic transition. In contrast, the HOMO–LUMO overlap, as observed from di-DCE-PBI (see Fig. 6(b)), hardly leads to electron density difference over the entire molecular framework, indicating that the ICT is substantially hindered in this case. Furthermore, considering the asymmetric PBIs (mono-Imi-mono-DCE-PBI and mono-Imi-mono-Imi$^+$-PBI), as indicated in Fig. 6(c) and (d), the variation in electron density around the bay substituents between the HOMO and LUMO levels resembles those in their corresponding symmetric counterparts and is not notably interfered by the presence of a different functional group at the opposite bay position.

Since the molecular orbital analysis suggests that ICT occurs and that the bay functional groups do not interact significantly with each other, this CT behaviour can be theoretically interpreted by a discrete component model, as illustrated in the schematic diagrams in Fig. 6. In this discrete component model, the structures of the bay-functionalized PBIs are divided into three separate parts: the PBI core and the two bay sub-stituents. Accordingly, the HOMO and LUMO energy levels of unsubstituted PBI are positioned in the centre, flanked by the energy levels of the two functional groups on both sides. Based on the excitation state analysis (see SI for details, in Section VI), the electronic transition from S_0 to S_1 for unsubstituted PBI mainly arises from the HOMO–LUMO transition. Therefore, we assume in this model that the energy levels of S_0 and S_1 can be directly correlated to HOMO and LUMO levels, respectively.

As demonstrated in Fig. 6, the PBI core acts as a photo-sensitiser that absorbs light to trigger the S_0–S_1 transition, promoting one of the two electrons from the HOMO level into the LUMO level. For the electron-rich Imi group, the HOMO level is higher than that of the PBI core, which makes electron transfer from the HOMO level of the Imi group to the HOMO level of the PBI core possible (illustrated by a black arrow in Fig. 6(a)). In contrast, the electron-deficient DCE group has a HOMO level lower than that of the PBI core, which prevents electron transfer from the DCE group to the PBI core (indicated by a red cross over the black arrow in Fig. 6(b)). Moreover, because the LUMO level of the DCE group is higher than that of the PBI core, electron transfer from the PBI core to the DCE group is also energetically unfavourable. As a result, the DCE group makes no contribution to electron transfer. Therefore, in the case of mono-Imi-mono-DCE-PBI, only electron transfer between the Imi group and the PBI core takes place *via* HOMO–HOMO interaction, as shown in Fig. 6(c).

To enable LUMO–LUMO interaction between the PBI core and the bay substituent, the functional group at the bay position should have a LUMO level lower than that of the PBI core. When di-Imi-PBI is partially protonated to form mono-Imi-mono-Imi$^+$-PBI, the positive charge at the bay position causes the LUMO level of the Imi$^+$ group to decrease below that of the PBI core. In the schematic diagram of mono-Imi-mono-Imi$^+$-PBI shown in Fig. 6(d), the HOMO–HOMO interaction between the neutral Imi species and the PBI core facilitates electron transfer. In addition, subsequent electron transfer becomes possible through the LUMO–LUMO interaction between the positively charged Imi$^+$ species and the PBI core. Consequently, the overall CT in mono-Imi-mono-Imi$^+$-PBI is much more pronounced than that in mono-Imi-mono-DCE-PBI.

The CT process typically opens up non-radiative decay pathways, so the number of photons returning to the ground state as fluorescence emission is reduced.[28] In this regard, a stronger CT effect results in more pronounced fluorescence quenching and therefore a lower PLQY. Back to the results from the titration assays, the minimal value of the PLQYs during the titration in CHCl$_3$ has been attributed to the formation of partially proto-nated mono-Imi-mono-Imi$^+$-PBI. Based on the discrete component model, this assignment can be now rationalized by the presence of an additional electron transfer from the LUMO level of the PBI core to the LUMO level of the Imi$^+$ moiety, in contrast to the electron transfer from the HOMO level of the Imi moiety to the HOMO level of the PBI core of unprotonated di-Imi-PBI. Furthermore, in the case of mono-Imi-mono-DCE-PBI, the DCE group introduces no electron transfer pathway, and the overall CT behaviour remains comparable to that of di-Imi-PBI. As a result, the PLQYs of mono-Imi-mono-DCE-PBI and di-Imi-PBI are not significantly different, as summarized in Table 1.

Conclusions

Starting from di-brominated perylene bisimides (PBIs), aldehyde groups were introduced at the bay positions following Suzuki coupling. Subsequently, benzimidazole (Imi) and dicyanoethy-lene (DCE) functionalities were introduced. Along with two symmetrically functionalized PBIs (di-Imi-PBI and di-DCE-PBI), an asymmetric one bearing Imi and DCE groups at opposite bay positions (mono-Imi-mono-DCE-PBI) was successfully synthe-sized. The absorption spectrum of this asymmetric PBI closely resembles that of di-DCE-PBI with two electron-withdrawing groups, while its emission spectrum aligns with that of di-Imi-PBI containing two electron-donating groups. Thus, the absorp-tion and emission properties of the asymmetric PBI are found to be influenced by the electron-withdrawing and electron-donating groups at the bay positions, respectively. Furthermore, acid titration assays with different solvent/acid combinations revealed a gradual conversion of di-Imi-PBI to its protonated species, in which the partially protonated mono-Imi-mono-Imi$^+$-PBI was involved. Remarkably, this asymmetric PBI intermediate exhibits the lowest photoluminescence quantum yield (PLQY), unlike its two symmetric counterparts. This is different to mono-Imi-mono-DCE-PBI, whose PLQY lies between those of its two symmetric counterparts. To rationalize these observations, a discrete com-ponent model treating the PBI core and the bay substituents independently was proposed. Theoretical calculations show that

23354 | *Phys. Chem. Chem. Phys.*, 2025, **27**, 23348–23355

This journal is © the Owner Societies 2025

the positively charged benzimidazolium (Imi$^+$) species has a lower LUMO level than the PBI core, allowing for additional electron transfer. As comparison, the higher LUMO level of the DCE group disfavours such transfer. This extra electron transfer in the partially protonated species accounts for the observed fluorescence quenching.

Author contributions

C. Meng: conceptualization, methodology, investigation, validation, visualization and writing – original draft, S. Eigler: conceptualization, resources, supervision and writing – review & editing.

Conflicts of interest

There are no conflicts to declare.

Data availability

Data for this article, including original data are available at refubium at **https://dx.doi.org/10.17169/refubium-47917**.

The data supporting this article have been included as part of the supplementary information (SI). Supplementary information is available. See DOI: **https://doi.org/10.1039/d5cp02789f**.

Acknowledgements

References

1 A. Nowak-Król, K. Shoyama, M. Stolte and F. Würthner, *Chem. Commun.*, 2018, **54**, 13763.

2 T. Li and X. Zhan, *Acta Chim. Sin.*, 2021, **79**, 257.

3 Z. Li, F. Liu, Y. Lu, J. Hu, J. Feng, H. Shang, B. Sun and W. Jiang, *ACS Catal.*, 2025, **15**, 1829.

4 D. Cappelletti, M. Barbieri, A. Aliprandi, M. Maggini and L. Dordevic, *Nanoscale*, 2024, **16**, 9153.

5 H. Langhals, *Helv. Chim. Acta*, 2005, **88**, 1309.

6 X. Zhang, C. Zhan, X. Zhang and J. Yao, *Tetrahedron*, 2013, **69**, 8155.

7 A. Böhm, H. Arms, G. Henning and P. Blaschka, *German Pat.*, DE 19547209A, 1997.

8 F. Würthner, V. Stepanenko, Z. Chen, C. Saha-Möller, N. Kocher and D. Stalke, *J. Org. Chem.*, 2004, **69**, 7933.

9 R. Dubey, A. Efimov and H. Lemmetyinen, *Chem. Mater.*, 2011, **23**, 778.

10 T. Ishi-i, K. Murakami, Y. Imai and S. Mataka, *Org. Lett.*, 2005, **7**, 3175.

11 P. Rajasingh, R. Cohen, E. Shirman, L. Shimon and B. Rybtchinski, *J. Org. Chem.*, 2007, **72**, 5973.

12 A. Nowak-Król and F. Würthner, *Org. Chem. Front.*, 2019, **6**, 1272.

13 S. Dey, A. Efimov and H. Lemmetyinen, *Eur. J. Org. Chem.*, 2012, 2367.

14 C. Chao, M. Leung, Y. Su, K. Chiu, T. Lin, S. Shieh and S. Lin, *J. Org. Chem.*, 2005, **70**, 4323.

15 S. Vajiravelu, R. Lygaitis, J. V. Grazulevicius, V. Gaidelis, V. Jankauskas and S. Valiyaveettil, *J. Mater. Chem.*, 2009, **19**, 4268.

16 V. Sivalmurugan, K. Kazlauskas, S. Jursenas, A. Gruodis, J. Simokaitiene, J. V. Grazulevicius and S. Valiyaveettil, *J. Phys. Chem. B*, 2010, **114**, 1782.

17 M. Hruzd, L. Rocard, A. Goujon, M. Allain, T. Cauchy and P. Hudhomme, *Chem. – Eur. J.*, 2020, **26**, 15881.

18 M. Luo and K. Chen, *Dyes Pigm.*, 2013, **99**, 456.

19 Z. Xie and F. Würthner, *Org. Lett.*, 2010, **12**, 3204.

20 H. Tsai and K. Chen, *J. Lumin.*, 2014, **149**, 103.

21 P. Rietsch, F. Witte, S. Sobottka, G. Germer, A. Krappe, A. Güttler, B. Sarkar, B. Paulus, U. Resch-Genger and S. Eigler, *Angew. Chem., Int. Ed.*, 2019, **58**, 8235.

22 K. Bahrami, M. M. Khodaei and I. Kavianinia, *Synthesis*, 2007, 547.

23 V. Campisciano, F. Giacalone and M. Gruttadauria, *ChemCatChem*, 2022, **14**, e202200696.

24 K. Gustav, M. Leonhardt and H. Port, *Monatsh. Chem.*, 1997, **128**, 105.

25 M. Oltean, A. Calborean, G. Mile, M. Vidrighin, M. Iosin, L. Leopold, D. Maniu, N. Leopold and V. Chis, *Spectrochim. Acta, Part A*, 2012, **97**, 703.

26 F. Fennel, S. Wolter, Z. Xie, P. Plötz, O. Kühn, F. Würthner and S. Lochbrunner, *J. Am. Chem. Soc.*, 2013, **135**, 18722.

27 M. Grabolle, R. Brehm, J. Pauli, F. M. Dees, I. Hilger and U. Resch-Genger, *Bioconjugate Chem.*, 2012, **23**, 287.

28 L. Ernst, H. Song, D. Kim and F. Würthner, *Nat. Chem.*, 2025, **17**, 767.

This journal is © the Owner Societies 2025

Phys. Chem. Chem. Phys., 2025, **27**, 23348–23355 | **23355**